ELSEVIER

International Journal of Mass Spectrometry 219 (2002) 305–313

International Journal of Mass Spectrometry

www.elsevier.com/locate/ijms

Field ionization and Coulomb explosion of methanol in an intense field of a femtosecond laser beam

Haizhen Ren, Chengyin Wu, Ri Ma, Hong Yang, Hongbing Jiang, Qihuang Gong*

State Key Laboratory for Mesoscopic Physics, Department of Physics, Peking University, Beijing 100871, PR China

Received 8 April 2002; accepted 27 May 2002

Abstract

Both mass spectra and photoelectron spectra of methanol were measured with a home-made time-of-flight (TOF) mass and photoelectron spectrometer under conditions with laser intensities varying from 7×10^{13} to 3×10^{15} W/cm^2, a wavelength centering at 810 nm, and a pulse duration of 110 fs. Differences were observed between the mass spectra when the laser polarization was parallel and orthogonal to the TOF axis, which were explained as the main contribution from the geometric alignment effect. We calculated the kinetic energy release (KER) from the Coulomb explosion of highly charged parent ion and discussed the possible channels based on the kinetic model. The angular distribution of the photoelectron is markedly anisotropic with a maximum when the laser polarization is parallel to the TOF axis. The kinetic energy of the photoelectron exhibits a featureless broad distribution extending above the laser's ponderomotive potential. These observations manifest that field ionization (FI) dominates under our experimental conditions. (Int J Mass Spectrom 219 (2002) 305–313)

Keywords: Coulomb explosion; Mass spectrum; Field ionization; Methanol; Femtosecond laser; Photoelectron spectrum

1. Introduction

The interaction of ultrafast, intense radiation with atomic and polyatomic systems has generated considerable interests [1–4], in part because the electric fields of the laser approach or even surpass the fields binding valance electrons to molecules. A detailed theoretical understanding of the interaction of such intense radiation with large molecules is difficult if not impossible due to the fact that the perturbation theory is inapplicable at such intense laser fields [5].

In 1964, Keldysh [6] suggested that field ionization (FI) could compete with a multiphoton ionization (MPI) process for atoms in an intense laser electric field. In Keldysh's theory a zero-range potential was employed to approximate the nuclear–electron interaction. DeWitt and co-workers [7–10] suggested a structure-based model to treat the FI of molecules and found that their model well explained the relative yields of various hydrocarbons.

The studies on the interaction of molecules with intense radiation mainly focus on the processes of dissociation, ionization, multiple ionization leading to Coulomb explosion and alignment in the field of laser pulse. At laser intensity of $\sim 10^{13}$ W/cm^2, intact parent ions in addition to dissociative fragments were observed in a 170 fs laser pulse at the central wavelength of 780 nm [7,11,12]. When the laser intensity is greater than 10^{15} W/cm^2, more than one electron may be removed from a molecule. Multiple charged molecules

* Corresponding author. E-mail: qhgong@pku.edu.cn

1387-3806/02/$ – see front matter
PII S1387-3806(02)00740-6

result and their Coulomb explosion, gives rise to the subsequent formation of fragment ions. The Coulomb explosions of diatomic and triatomic molecules include: H_2 [13,14], N_2 [15–18], O_2 [18], I_2 [19,20], CO_2 [16,21], and NO_2 [22]; they have been extensively studied. The kinetic energies of formed fragment ions are substantially lower than that expected for prompt ionization/dissociation at the equilibrium bond length which can be explained by a kinetic model based on an explosion at a critical distance [23]. Large clusters in an intense femtosecond laser field have been found to produce much more energetic particles and to behave like a microplasma [24]. Polyatomic molecules can be classified as an intermediate case between two- or three-atom molecules and large clusters. Coulomb explosion for large polyatomic molecules have been observed including C_{60} [25], benzene [26], and SF_6 [27].

In addition to the mass spectrum, the photoelectron spectrum (PES) is also a useful tool to elucidate the ionization and dissociation process of molecules in an intense laser field. The photoelectrons contain much dynamic information about the ionization and dissociation process and are helpful to explain clearly the ionization and dissociation process. In the case of MPI, a limited number of features displaying the periodicity of the photon energy can be observed. A PES displaying a featureless distribution extending above the laser's ponderomotive potential is a hallmark of the FI regime. Mevel et al. [28] used photoelectron spectroscopy to observe a transition from MPI to FI in a series of noble gas atoms ranging from Xe to He. The transition was apparent in the fact that there were distinct MPI/ATI features observed in Xe spectrum and the MPI/ATI features gradually disappeared as the ionization potential was increased through the series of target gases including Kr, Ar, Ne, and He. A similar transition from the multiphoton to FI regime has also been observed in the series of aromatic molecules like benzene naphthalene and anthracene [8].

In this work, we describe the ionization and dissociation of methanol molecule at laser intensities covering the range of $7 \times 10^{13} \sim 3 \times 10^{15}$ W/cm^2 using a TOF mass and photoelectron spectrometer. The kinetic energies of fragment ions originating from Coulomb explosion were measured and the explosion

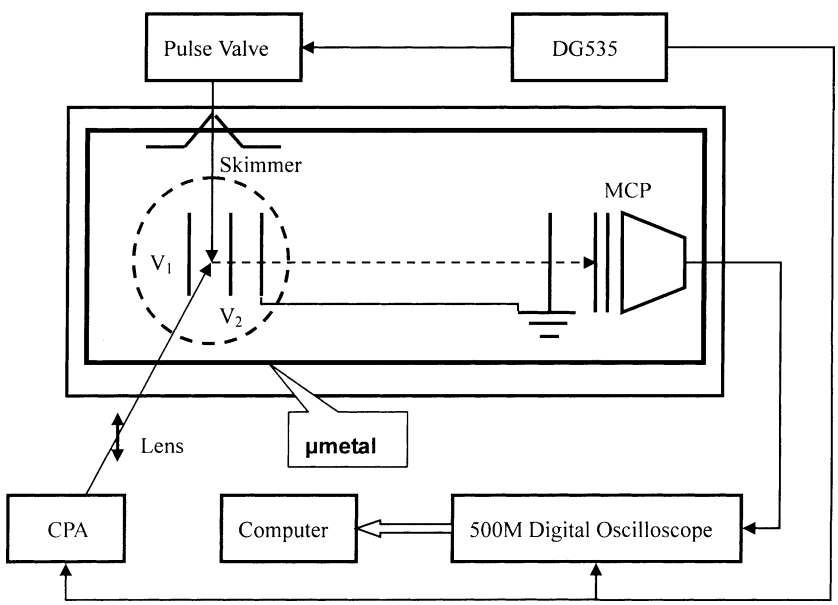

Fig. 1. Schematic diagram of the home-built TOF mass and photoelectron spectrometer. The timing schedules of the general pulsed valve, CPA laser and the sampling oscilloscope were controlled by a DG535 digital delay.

channels will be discussed. The kinetic energy distribution and angular distribution of the photoelectrons were also measured.

2. Experimental

A Ti:Sapphire chirped pulse amplifier (CPA) laser system (TSA-10, Spectra-Physics Inc., USA), which delivered 810 nm, 110 fs at a repetition of 10 Hz, was employed as the light source. The maximum output is 10 mJ per pulse. The amplified laser beam was focused into the chamber of the TOF mass spectrometer with a 150 mm focal length lens. To measure the angular distribution, a half-wave plate was inserted into the path of the laser beam to rotate the electric field vector.

The schematic diagram of the experimental system is shown in Fig. 1, which has been described in define in previous work [29]. The inner-wall of the entire vacuum chamber was wrapped with μ-metal to shield the geomagnetism. The vapor from liquid methanol was introduced into the chamber via a pulsed valve (Park Inc., USA) with a 0.2 mm orifice. The chamber pressure was maintained at several 10^{-4} Pa to avoid space–charge effect and pressure broadening of the ion peaks. This system employed a dual slope extraction field. The distance between the V_1 and V_2 plate was 10 mm. The charged particles were extracted to the field-free drift tube with a length of 35 cm. A microchannel plate assembly was used to detect the ions or photoelectrons. The signals were recorded using a digital oscillator with a 500 MHz sampling rate (H-P, USA) and were typically averaged over 256 cycles. The data were then transferred to a PC for storage and analysis.

3. Results and discussion

3.1. Ion spectroscopy

Fig. 2 shows the TOF mass spectra of methanol obtained at intensity of 3×10^{15} W/cm^2. The extraction voltages for the V_1 and V_2 plates were 960 and 800 V, respectively. The laser polarization direction was parallel to the drift tube axis for the upper trace and orthogonal for the lower trace. Abundant signals of fragment ions H^+, C^{m+} ($m = 1, 2, 3$) and O^{n+} ($n =$

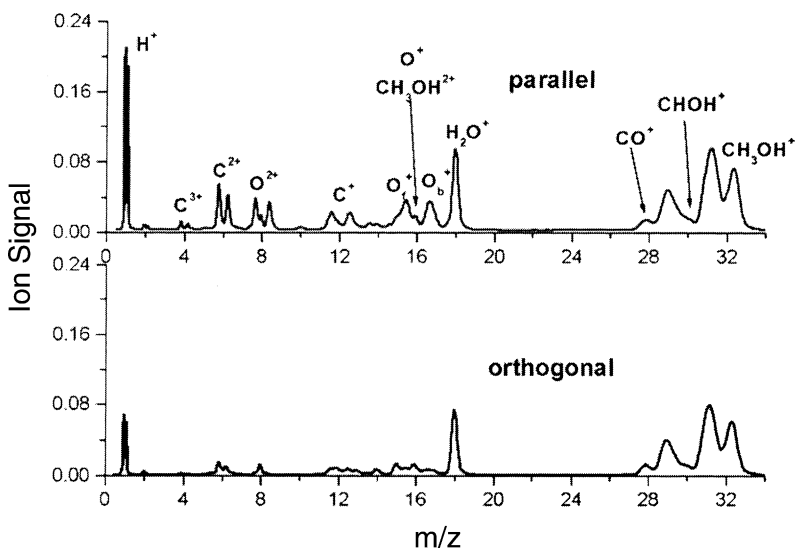

Fig. 2. TOF mass spectra of methanol induced by 810 nm, 110 fs laser pulses at the intensity of 3×10^{15} W/cm^2. The extraction voltages of the V_1 and V_2 plates are 960 and 800 V, respectively. The laser polarization is parallel in the upper trace and orthogonal in the lower trace to the TOF axis. The H_2O^+ signal at a high intensity originated from a background gas.

1, 2) were observed. It was noted that the signals of fragment ions of the parallel case are larger than that of the orthogonal case. The differences between these two cases can be attributed to two effects: dynamic alignment and geometric alignment. In the dynamic alignment mechanism, the electric field of the intense laser induces a polarization within the molecule which in turn interacts with the field. Consequently, this sets up a torque which acts to align the molecule axis with the field. As for the geometric alignment mechanism, the dependence of the ionization rate on the angle between the laser polarization direction and the linear molecular axis determines the angular distribution of the exploding fragments [30]. By measuring the ratio of fragment ion yields obtained at a parallel polarization vs. on orthogonal polarization a range of laser intensities, we can distinguish between the effect of dynamic alignment and geometric alignment [31]. Fig. 3 depicts the laser intensity dependence of the ratio of $C_{\parallel}^{m+}/C_{\perp}^{m+}$ ($m = 1, 2, 3$) and $O_{\parallel}^{n+}/O_{\perp}^{n+}$ ($n = 1, 2$), where the subscripts $\parallel$ and $\perp$ denote, respectively, the C^{m+} (or O^{n+}) yield when the laser polarization direction is parallel and orthogonal to the axis of the TOF mass spectrometer. As a stronger laser field can induce larger dipole moment, the degree of dynamic alignment will increase with laser intensity. In other words, the ratio of $\parallel/\perp$ will increase with increasing laser intensity for dynamic alignment. As for the geometric alignment, the ionization probability depends on the angle between the laser polarization direction and the molecule axis. The ionization probability reaches maximum for the molecules with axis parallel to the laser polarization direction. If the laser intensity is strong enough, the ionization probability remains unchanged for molecules with axis parallel to the laser polarization direction. In contrast, the probability still increases with laser intensity for the molecules with axis normal to the laser polarization direction. Consequently, the ratio of $\parallel/\perp$ will shrink with increasing laser intensity. In our result, an overall drop occurs for both the $C_{\parallel}^{m+}/C_{\perp}^{m+}$ and $O_{\parallel}^{n+}/O_{\perp}^{n+}$ ratios as the laser intensity is increased from 10^{13} to 10^{15} W/cm^2. These observations suggest that a geometric alignment is responsible for the anisotropic angular distribution of the exploding fragments.

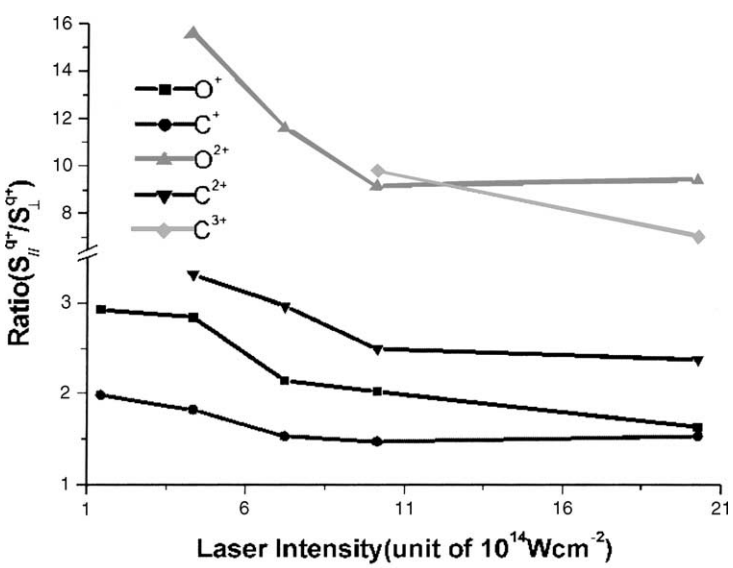

Fig. 3. Variation with laser intensity of the ratio of $C_{\parallel}^{m+}/C_{\perp}^{m+}$ (and $O_{\parallel}^{n+}/O_{\perp}^{n+}$) $\parallel$ and $\perp$ denote, respectively, the ion yield when the laser polarization is parallel and orthogonal to the TOF axis.

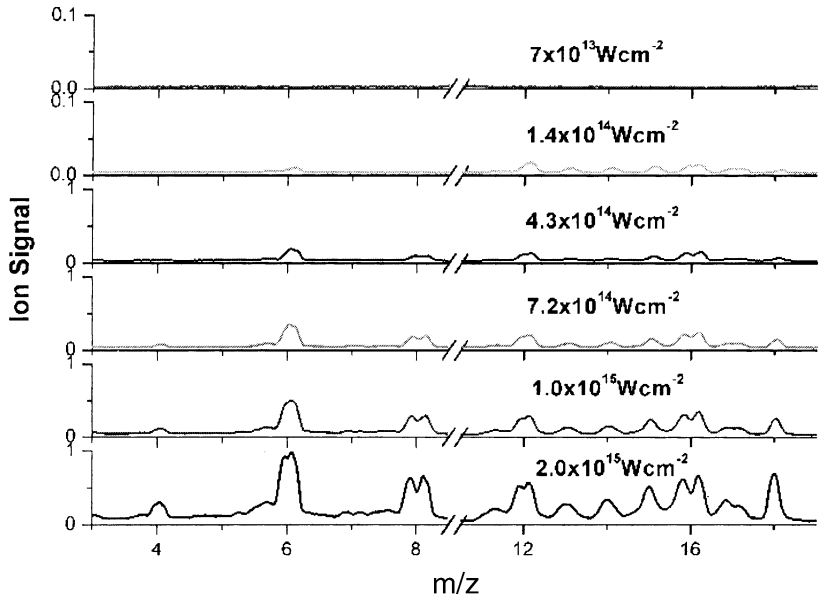

Fig. 4. Part of TOF spectra for methanol at six different laser intensities ranging from 7×10^{13} to 2×10^{15} W/cm^2. The laser polarization direction is parallel to the TOF axis. The extraction voltages of the V_1 and V_2 plates are 1400 and 800 V, respectively.

For the parallel polarization case, part of the TOF spectra of methanol molecule are shown in Fig. 4 at laser intensities ranging from 7×10^{13} to 2×10^{15} W/cm^2. At an intensity of 7×10^{13} W/cm^2, we could hardly observe any obvious signal of fragment ions. When the laser intensity is increased, the fragment ion signals appear and split into double peaks which indicate that a Coulomb explosion has occurred. The kinetic energy release in the process of Coulomb explosion causes the ion signal to display peak splitting. The peak with a shorter flight-time arises from ions ejected along the axis of the TOF mass spectrometer directly towards the detector and peak with a longer flight-time from ions ejected in the opposite direction.

The kinetic energy release (KER) from the Coulomb explosion can be determined from the peak splitting observed for multiply charged ions according to [32]

$$E_{\text{kinetic energy}} = \frac{(U_1 - U_2)^2}{8md^2} q^2 \Delta t^2 \quad (1)$$

where U_1 is the potential of the repeller plate, U_2 the potential of the first acceleration plate, d the distance between these two plates, q the charge of the ion and Δt is the difference in arrival times between forward and backward ejected ions. Fig. 5 shows the average kinetic energies of C^{m+} and O^{n+} at laser intensities ranging from 1.4×10^{14} to 2.0×10^{15} W/cm^2. It is noted that the average kinetic energies increase with increase of laser intensity. The measured kinetic energy of fragment ions originated from Coulomb repulsion energy of highly charged methanol ion. The Coulomb repulsion energies are determined by the following equation [33]:

$$E = 14.4 \frac{q_1 q_2}{r} \quad (2)$$

where q_1 and q_2 are the ions' charge (e), r the distance between the ions (Å), and the calculated result is in unit of eV. In Table 1, the average kinetic energies of C^{m+} and O^{n+} ions after Coulomb explosion at laser intensity of 2×10^{15} W/cm^2 are listed. The molecular structure of methanol is shown in Fig. 6. Since the mass of C and O is much larger than that of H, we can simply choose the C–O bond as the molecular axis. Coulomb explosion channels in this assumption

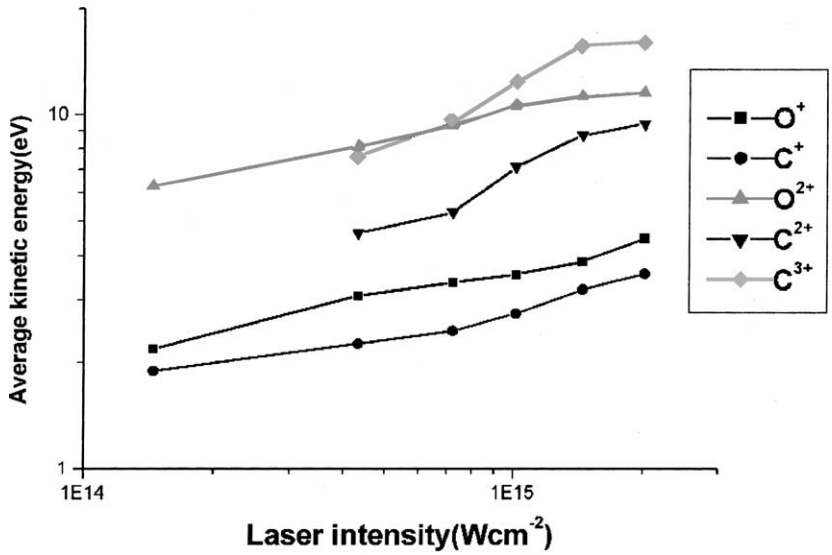

Fig. 5. Variation of average kinetic energies of C^{m+} and O^{n+} determined by the peak method splitting with laser intensity.

are expressed by (m, n) and are given by

$$CH_3OH \rightarrow [CH_3OH]^{(m+n+4)+}$$
$$\rightarrow C^{m+} + O^{n+} + 4H^+ + KER$$

One of the most important features in the Coulomb explosion of small molecules is that the measured kinetic energy releases are generally weaker than the expected Coulomb repulsion energy starting at the equilibrium internuclear distance R_e of the neutral molecules. It has been suggested that the Coulomb explosion begins at a critical internuclear distance R_c larger than R_e; for small molecules, R_c is about a factor of two larger than R_e [26,35,36]. Since the KER originates from the Coulomb repulsion energy of charged particles in parent ion, the value of E_{exp}/E_{Coul} couldn't be larger than unity. The most feasible channels are those whose value of E_{exp}/E_{Coul} are about 50% due to the $1/R$ dependence of the Coulomb repulsion potential. Thus, the channel of

Table 1
Observed kinetic energy (E_{exp}) at an intensity of 2×10^{15} W/cm^2 and the calculated Coulomb repulsion energy (E_{Coul}) at the equilibrium structure of the methanol molecule

Ions	Channels (m, n)	E_{exp} (eV)	E_{Coul} (eV)	E_{exp}/E_{Coul} (%)
C^+	(1, 1)	3.56	6.07	59
	(1, 2)	3.56	11.81	30
C^{2+}	(2, 1)	9.40	12.14	77
	(2, 2)	9.40	23.62	40
C^{3+}	(3, 1)	16.03	18.22	88
	(3, 2)	16.03	35.43	45
O^+	(1, 1)	4.47	5.14	87
	(2, 1)	4.47	9.44	47
	(3, 1)	4.47	13.74	33
O^{2+}	(1, 2)	11.52	10.27	112
	(2, 2)	11.52	18.88	61
	(3, 2)	11.52	27.49	42

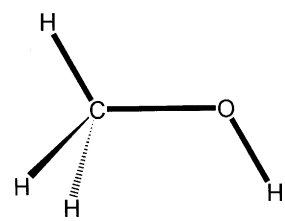

Fig. 6. The molecular structure of methanol. The bond length of HC, CO, and OH are 1.12, 1.37, and 1.04 Å, respectively. The angle of HCH, HCO, and COH are 108.2°, 110.7°, and 107.3°, respectively. These data are taken from [34].

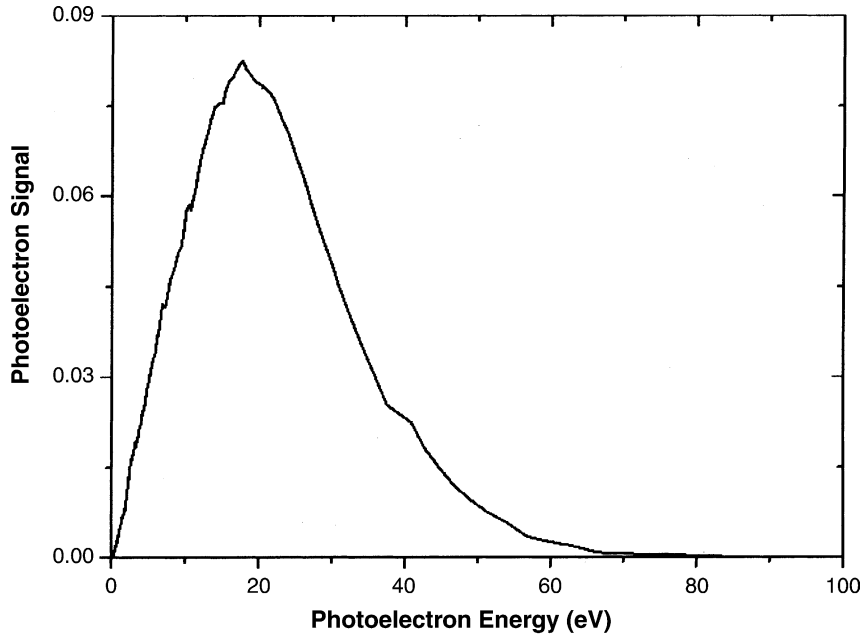

Fig. 7. Photoelectron spectra of methanol measured at 2×10^{15} W/cm^2. The voltages of V_1 and V_2 plate are both zero.

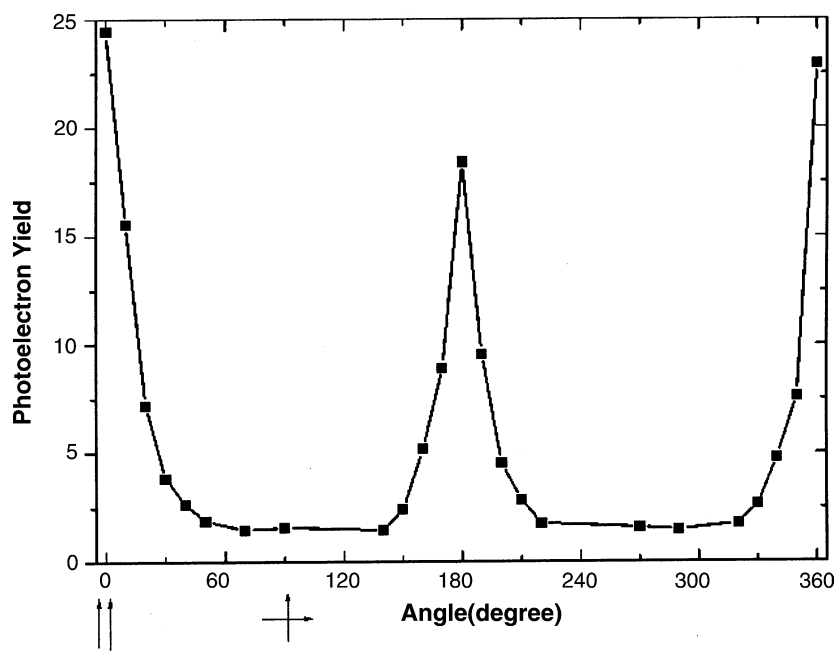

Fig. 8. Angular distribution of the photoelectrons at a laser intensity of 2×10^{15} W/cm^2.

(1, 2) contribute little to the yield of ion O^{2+} because its value of E_{exp}/E_{Coul} is larger than unity. The most feasible channel for ion O^{2+} is (2, 2) and (3, 2).

3.2. PES

The PES of methanol is shown in Fig. 7 at a laser intensity of 2×10^{15} W/cm^2. The voltages of the V_1 and V_2 plates were both set to zero. There are no discernible features other than a broad distribution extending above the laser's ponderomotive potential U_p which reads [23]:

$$U_p = \frac{e^2 E_0^2}{4m\omega^2} = 9.33 \times 10^{-14} I_0 \lambda^2, \quad (3)$$

where E_0 is the laser field strength, I_0 the laser intensity (W/cm^2), λ the wavelength (μm), and the calculated result is in unit of eV. Under our experimental conditions, the value of U_p is estimated to be several tens of eV.

According to the FI model [37], the photoelectrons were produced by two steps. Firstly, the electrons are considered to be ionized through tunneling to near-zero kinetic energy states. Second, the classical electrons are accelerated by the still-present strong electric field. As the tunneling time of electron through the barrier formed by the molecule potential and the laser electric field is indeterminate, the kinetic energy of the electron in an ac linear electric field is indeterminate, too. This agrees with our measured photoelectron kinetic spectrum that exhibits a featureless broad distribution.

Fig. 8 shows the angular distribution of the photoelectron at the laser intensity of 2×10^{15} W/cm^2. It is obvious that the photoelectron distribution is markedly anisotropic and reaches a maximum when the laser polarization direction is parallel to the TOF axis. This fact can be interpreted by a FI mechanism. The photoelectron gained momentum during the vibration process forced by the laser electric field. As a result, the momentum of the photoelectron mainly distributes along the laser polarization direction. So the photoelectron had maximal intensity when the laser polarization is parallel to the TOF axis.

4. Conclusions

FI and Coulomb explosions of polyatomic methanol molecule induced by intense femtosecond laser beams at intensities varying from 7×10^{13} to 3×10^{15} W/cm^2 were experimentally investigated. According to the measured kinetic energy of fragment ions from Coulomb explosion, we discussed the Coulomb explosion pathways. The geometric alignment was found to be responsible for the anisotropic angular distribution of the exploding fragment ions. The angular distribution and kinetic energy distribution of the photoelectron reveal that the FI dominates under our experimental conditions.

Acknowledgements

This work was supported by the National Key Basic Research Special Foundation (NKBRSF) under Grant No. G1999075207, National Natural Science Foundation of China under Grant No. 19884001, 10104003 and 90101027.

References

[1] S.M. Hankin, D.M. Villeneuve, P.B. Corkum, D.M. Rayner, Phys. Rev. Lett. 84 (2000) 5082.
[2] R.J. Levis, G.M. Menkir, H. Rabitz, Science 292 (2001) 709.
[3] C.Y. Wu, et al., J. Phys. Chem. A 105 (2001) 374.
[4] C.Y. Wu, Q.H. Gong, Chin. Phys. 10 (2001) 814.
[5] D. Bauer, R. Mulser, Phys. Rev. A 59 (1999) 569.
[6] L.V. Keldysh, Sov. Phys. JETP 20 (1965) 1307.
[7] M.J. DeWitt, R.J. Levis, J. Chem. Phys. 108 (1998) 7045.
[8] M.J. DeWitt, R.J. Levis, Phys. Rev. Lett. 81 (1998) 5101.
[9] M.J. DeWitt, R.J. Levis, J. Chem. Phys. 110 (1999) 11368.
[10] B.S. Prall, M.J. DeWitt, R.J. Levis, J. Chem. Phys. 111 (1999) 2865.
[11] M.J. DeWitt, R.J. Levis, J. Chem. Phys. 102 (1995) 8670.
[12] M.J. DeWitt, D.W. Peters, R.J. Levis, Chem. Phys. 218 (1997) 211.
[13] G.N. Gibson, M. Li, C. Guo, J. Neira, Phys. Rev. Lett. 79 (1997) 2022.
[14] M.R. Thompson, M.K. Thomas, P.F. Taday, J.H. Posthumus, A.J. Langley, L.J. Frasinski, K. Codling, J. Phys. B: Atom. Mol. Opt. Phys. 30 (1997) 5755.
[15] L.J. Frasinski, K. Codling, P.A. Hatherly, Phys. Lett. A 142 (1989) 499.
[16] P. Hering, C. Cornaggia, Phys. Rev. A 59 (1999) 2836.

[17] A. Hishikawa, A. Iwamae, K. Hoshina, M. Kono, K. Yamanouchi, Chem. Phys. 231 (1998) 315.
[18] C.L. Guo, M. Li, G.N. Gibson, Phys. Rev. Lett. 82 (1999) 2492.
[19] C. Ellert, P.B. Corkum, Phys. Rev. A 59 (1999) R3170.
[20] P.A. Hatherly, M. Stankiewicz, K. Codling, L.J. Frasinski, G.M. Cross, J. Phys. B: Atom. Mol. Opt. Phys. 27 (1994) 2993.
[21] P. Graham, K. Ledingham, R.P. Singhal, T. McCanny, S.M. Hankin, J. Phys. B: Atom. Mol. Opt. Phys. 32 (1999) 5557.
[22] P. Graham, K.W.D. Ledingham, R.P. Singhal, T. McCanny, S.M. Hankin, X. Fang, P. Tzalllas, C. Kosmidis, P.F. Taday, A.J. Langley, J. Phys. B: Atom. Mol. Opt. Phys. 33 (2000) 3779.
[23] N. Nakashima, et al., J. Photochem. Photobiol. C: Photochem. Rev. 1 (2000) 131.
[24] C. Lifshitz, Int. J. Mass Spectrom. 200 (2000) 423.
[25] R.C. Constantinescu, S. Hunsche, H.B. van Linden, van den Heuvell, H.G. Muller, Phys. Rev. A 58 (1998) 4637.
[26] S. Shimizu, J. Kou, S. Kawato, K. Shimizu, S. Sakabe, N. Nakashima, Chem. Phys. Lett. 317 (2000) 609.
[27] J.H. Sanderson, R.V. Thomas, W.A. Bryan, W.R. Newell, P.F. Taday, A.J. Langley, J. Phys. B: Atom. Mol. Opt. Phys. 30 (1997) 4499.
[28] E. Mevel, R. Breger, R. Trainham, G. Petite, P. Agostini, Phys. Rev. Lett. 70 (1993) 406.
[29] C.Y. Wu, H.Z. Ren, T.T. Liu, R. Ma, H. Yang, H.B. Jiang, Q.H. Gong, Int. J. Mass. Spectrom. 216 (2002) 249.
[30] J.H. Posthumus, J. Plumridge, M.K. Thomas, K. Codling, L.J. Frasinski, A.J. Langley, P.F. Taday, J. Phys. B: Atom. Mol. Opt. Phys. 31 (1998) L553.
[31] S. Banerjee, G. Ravindra Kumar, D. Mathur, Phys. Rev. A 60 (1999) R3369.
[32] L. Poth, Q. Zhong, J.V. Ford, S.M. Hurley, A.W. Castleman Jr., Chem. Phys. 239 (1998) 309.
[33] L. Adoui, C. Caraby, A. Cassimi, D. Lelièvre, G.P. Grandin, A. Dubois, J. Phys. B: Atom. Mol. Opt. Phys. 32 (1999) 631.
[34] E.V. Svash, D.M. Dennison, J. Chem. Phys. 21 (1957) 1804.
[35] C. Cornaggia, M. Schmidt, D. Normand, Phys. Rev. A 51 (1995) 1431.
[36] C. Cornaggia, Phys. Rev. A 52 (1995) R4328.
[37] M.J. Nandor, M.A. Wallker, L.D. Van Woerkom, J. Phys. B: Atom. Mol. Opt. Phys. 31 (1998) 4617.